communications earth & environment

Article

A Nature Portfolio journal

https://doi.org/10.1038/s43247-026-03186-8

Cumulative hydrodynamic impacts of offshore wind farms on North Sea currents and surface temperatures

Nils Christiansen [1] ✉, Ute Daewel [1] & Corinna Schrum [1,2]

Offshore wind farms are increasingly shaping coastal ocean dynamics, yet their cumulative physical impacts remain poorly quantified. Using decade-long, high-resolution simulations of the North Sea, we show that large-scale offshore wind development can reduce current velocities by up to 20% and reshape local tidal energy distributions. Wind and tidal wakes exert distinct but interacting influences on ocean physics: wind speed anomalies drive far-field hydrodynamic impacts, while structure-induced drag intensifies local turbulence and mixing. Turbine spacing emerges as a key control on wake interactions, governing the formation of high-turbulence hotspots. The near- and far-field wake effects affect vertical mixing and surface heat fluxes – primarily driven by large-scale wind stress reductions – leading to shallower mixed layers and long-term surface warming of up to 0.2 °C in wind farm areas. Our findings reveal a basin-scale physical footprint of offshore wind energy and highlight the need to account for hydrodynamic impacts in future offshore wind farm planning.

The North Sea is a dynamic shelf sea, strongly influenced by wind and tidal forces and characterized by seasonal stratification. Its physical environment plays a critical role in driving biogeochemical cycles and shaping the dynamics of lower trophic ecosystems. As a result, disturbances to these natural processes can fundamentally affect the marine environment. By 2024, ~23.5 GW of offshore wind energy had been installed in the North Sea, with around 4500 turbines in operation. With political targets aiming to increase capacity to 120 GW by 2030 and 300 GW by 2050[1], the anticipated growth in offshore wind installations in the North Sea raises concerns about potential systematic hydrodynamic changes in areas designated for intensive development.

Drag from offshore wind turbine installations—both in the atmosphere and the ocean—has been shown to influence ocean dynamics at local to regional scales, leaving an impact on the marine environment. Designated to harvest energy from the wind field over the sea, wind turbines reduce the kinetic wind energy at hub height and create a downstream momentum deficit. This deficit is characterized by high turbulence from horizontal wind shear and wind speeds up to 40% lower than the ambient wind field[2–7]. These atmospheric wake structures propagate both laterally and vertically behind offshore wind farms (OWFs), reaching the sea surface at distances of approximately ten rotor diameters[8]. Observations in the North Sea have shown that near-surface wakes can extend up to 100 km downstream of large turbine clusters, depending on wind farm properties and atmospheric stability[5,9,10]. At the same time, wind wakes reduce surface winds by around $10-15\%$ compared to undisturbed conditions[9–11]. Consequently, wind wakes affect the air-sea boundary layer, with implications for sea surface climate[12], surface currents, and mixing[13]. The latter has been associated with upwelling and downwelling patterns that influence vertical transport and sea surface elevation[14–18]. In this context, tides were found to play a decisive role in modulating the magnitude of the emerging hydrodynamic changes[18].

Below sea surface, pile structures like monopile foundations form an additional underwater drag on the tidal currents, which influences horizontal flow velocities and produces high turbulence in direct vicinity of the turbine sites[19–24]. These tidal wakes emerge on much smaller scales than wind wakes and extend a few hundred meters to kilometers downstream of the pile structures[25–27]. The local shear effects were found to double seabed drag coefficients[24] behind the wind turbines and create strong but site-specific vertical mixing that can exceed natural mixing and reduce vertical gradients in the water column like vertical temperature stratification[28–30]. Recent model simulations indicated that for shallow North Sea water conditions the drag of densely built-up wind farms can lead to blocking effects on mean tidal currents[31] and reduce the local current velocities by around 5% [32].

Although wind- and tide-generated wakes originate at different spatial scales, both can modify tidal and density currents, vertical mixing, and density stratification far beyond wind farm boundaries[13,18,32,33]. The local wake effects accumulate in regions with dense offshore wind development, thereby altering hydrodynamic processes in the far field. Previous modeling

[1]Institute of Coastal Systems – Analysis and Modeling, Helmholtz-Zentrum Hereon, Geesthacht, Germany. [2]Institute of Oceanography, Universität Hamburg, Hamburg, Germany. ✉e-mail: nils.christiansen@hereon.de

studies have found that OWFs can cause large-scale destratification in the German Bight due to monopile-induced mixing[32], and have demonstrated hydrodynamic changes extending over hundreds of kilometers as a result of wind speed reductions caused by turbine installations in the North Sea[13,18]. These physical alterations not only influence regional ocean dynamics of the North Sea but have also been linked to changes in biogeochemical processes within the marine ecosystem[30,33,34]. Despite the detailed analyzes existing in today's literature, however, the combined effects of wind and tidal wakes remain largely unexplored, and their long-term impacts are still insufficiently understood.

In this study, we address these knowledge gaps by exploring the cumulative impacts of OWFs on the hydrodynamics of the central and southern North Sea. Our primary objective is to understand how wind and tidal wakes interact to influence regional hydrodynamics, while also evaluating the cumulative, long-term changes resulting from large-scale offshore wind energy expansion. In particular, we aim to identify the dominant processes driven by the OWF wakes and examine both local and far-field effects. For this purpose, we deploy three-dimensional regional hydrodynamic modeling with unstructured grids and parameterize the subgrid drag effects above and below the sea surface at wind turbine sites.

The study is structured into two parts. In the first part, we examine the present state of offshore wind expansion (2023; Supplementary Fig. 1a) to investigate the synergistic and antagonistic interactions between wind and tidal wakes in an environment relatively sparsely covered by OWFs. This analysis provides a baseline understanding of the dominant processes associated with the superposition of wind and tidal wakes. In the second part, we assess how North Sea hydrodynamics may change in the long term under the cumulative impacts of rotor-induced wind drag and monopile-induced mixing, focusing on a large-scale offshore wind scenario for 2050 (Supplementary Fig. 1b).

Our model simulations indicate that future offshore wind expansion may strongly influence hydrodynamic conditions across the North Sea. We identify large-scale reductions in residual current velocities, changes in shear-induced mixing, bottom stress, and stratification. The model simulations suggest persistent surface warming in wind farm areas, reaching up to 0.2 °C, which is strongly driven by the reductions in surface wind stress, affecting surface layer mixing and heat fluxes. At the same time, localized turbulence hotspots from tidal wakes can increase vertical mixing and partially erode summer stratification, thereby counteracting some of the basin-scale effects. Eventually, wind and tidal wakes prove to be considerable anthropogenic physical drivers in the North Sea, with potentially wide-ranging implications for nutrient cycling, primary productivity, and marine ecosystem dynamics.

Results and discussion

Hydrodynamic footprints of wind and tidal wakes

Wind wakes and tidal wakes have been shown to affect horizontal flow and turbulent motion in the vicinity of OWF sites. However, their impacts on the water column unfold differently. A comparison of the two effects is depicted in Fig. 1, showing the individual and cumulative impacts on surface current velocities and surface turbulent kinetic energy, averaged over a period of 6 years.

Recent studies have demonstrated that wind and tidal wakes reduce mean current velocities by either decreasing wind-induced shear or obstructing horizontal currents. Our model simulations reveal large-scale reductions in mean surface current velocity of around 10% due to wind wakes (Fig. 1a), closely aligning with previous findings[13,33]. Meanwhile, tidal wakes have approximately half the impact, causing mean velocity changes of about 5% (Fig. 1b), consistent with previous estimates of monopile-induced current reductions[18,31]. Despite differences in magnitude, both wake effects similarly influence mean tidal currents and attenuate downstream flow velocities tens of kilometers along the prevailing horizontal flow, while increasing velocities on the sides of the wind farms (Fig. 1c). Overall, the impact on mean surface velocity is primarily driven by wind speed reductions and amplified locally by monopile drag, resulting in changes of up to 20% or more in areas with multiple wind turbine clusters (Fig. 1c).

In contrast to their impact on current velocity, wind and tidal wakes have opposing effects on turbulent kinetic energy (TKE) in the water. The reduction in surface wind stress caused by wind wakes decreases vertical shear in surface layers, thereby attenuating surface TKE near OWFs (Fig. 1d). Reflecting the changes in surface wind speed, the impact on mean TKE extends several kilometers beyond the boundaries of the wind farms, with the strongest reductions of around $5-10\%$ occurring close to the wind farm sites. Conversely, tidal wakes caused by friction at the monopile foundations generate strong increases in surface TKE and throughout the water column (Fig. 1e). The elevated TKE levels remain localized around the turbine locations, which is in agreement with recent in-situ measurements[24,29]. With magnitudes of more than 30%, the monopile-induced changes can be an order of magnitude greater than the simulated wind wake effects and, in some cases, exceed ambient turbulence levels. As a result, we find that the combined effect of wind and tidal wakes is characterized by local hotspots of strong TKE generation, surrounded by broader areas of attenuated surface layer turbulence (Fig. 1f).

The emerging TKE changes at OWFs appear to be site-specific, influenced by factors such as turbine spacing, water depth, and local hydrodynamics conditions, all of which contribute to the intensity and accumulation of additional turbulence generation. For instance, the model shows increasing TKE changes as wind farms are situated closer to the coast, where tidal velocities are higher, and reveals variations between neighboring wind farms with different turbine densities (Fig. 1e, f). Previous studies have already suggested links between the turbine spacing and the impact of OWFs[31,35]. Here, the extent of TKE generation appears dependent on turbine spacing, thereby determining whether additional TKE is sufficient to counteract the TKE attenuation from reduced wind stress. It should be noted, however, that this attenuation by wind wakes occurs primarily in the wind-driven surface layers, while the monopile effects generally remain dominant in deeper layers. Additionally, the impact of wind wakes itself could decrease by building larger turbines with larger spacings[35], which is not considered here.

Given the alterations in turbulent motion, wind and tidal wakes influence water column mixing at wind farm sites, primarily driven by the high turbulence levels generated by tidal wakes. As an example, we illustrate the mean annual cycle of changes in near-surface vertical eddy diffusivity K_v, as a measure for vertical mixing, and sea surface temperature SST at the location of the FINO1 research platform in the German Bight (Fig. 2a, b).

Tidal wakes increase annual surface mixing rates by $0.005-0.010\,m^2s^{-1}$ (Fig. 2a), corresponding to an intensification of $50-100\%$ in winter (ambient rates around $0.01-0.02\,m^2s^{-1}$) and over 100% during summer (ambient rates down to $0.0005\,m^2s^{-1}$). These results are consistent with in-situ observations[24], showing an increase in water column mixing by about one order of magnitude. The impact on near-surface K_v itself follows a seasonal trend, with higher amplitudes in autumn and winter, likely related to variations in the drag force with the ambient turbulence intensity and tidal current velocities. In contrast, the influence from wind wakes is an order of magnitude smaller and barely contributes to the overall impact at FINO1. Still, a seasonal trend can be observed here as well, with weaker effects during summer and stronger reductions in winter due to higher prevailing wind speeds and thus stronger reductions in wind-induced turbulence.

The altered vertical mixing rates are directly linked to changes in SST and temperature stratification (Fig. 2b, c). Tidal wakes enhance turbulent mixing, bringing colder bottom waters to the warmer surface and lowering SST in summer by up to 0.5 °C. Their influence is strongest between March and September, whereas in winter the well-mixed water column minimizes the effect of structure-induced mixing. In contrast, wind wakes reduce surface wind stress, attenuating surface layer mixing and limiting heat exchange with the atmosphere, which causes SST to rise by up to 0.2 °C (Fig. 2b). Wind wakes affect the air-sea exchange and SST throughout the year, but the strongest temperature changes occur during periods when

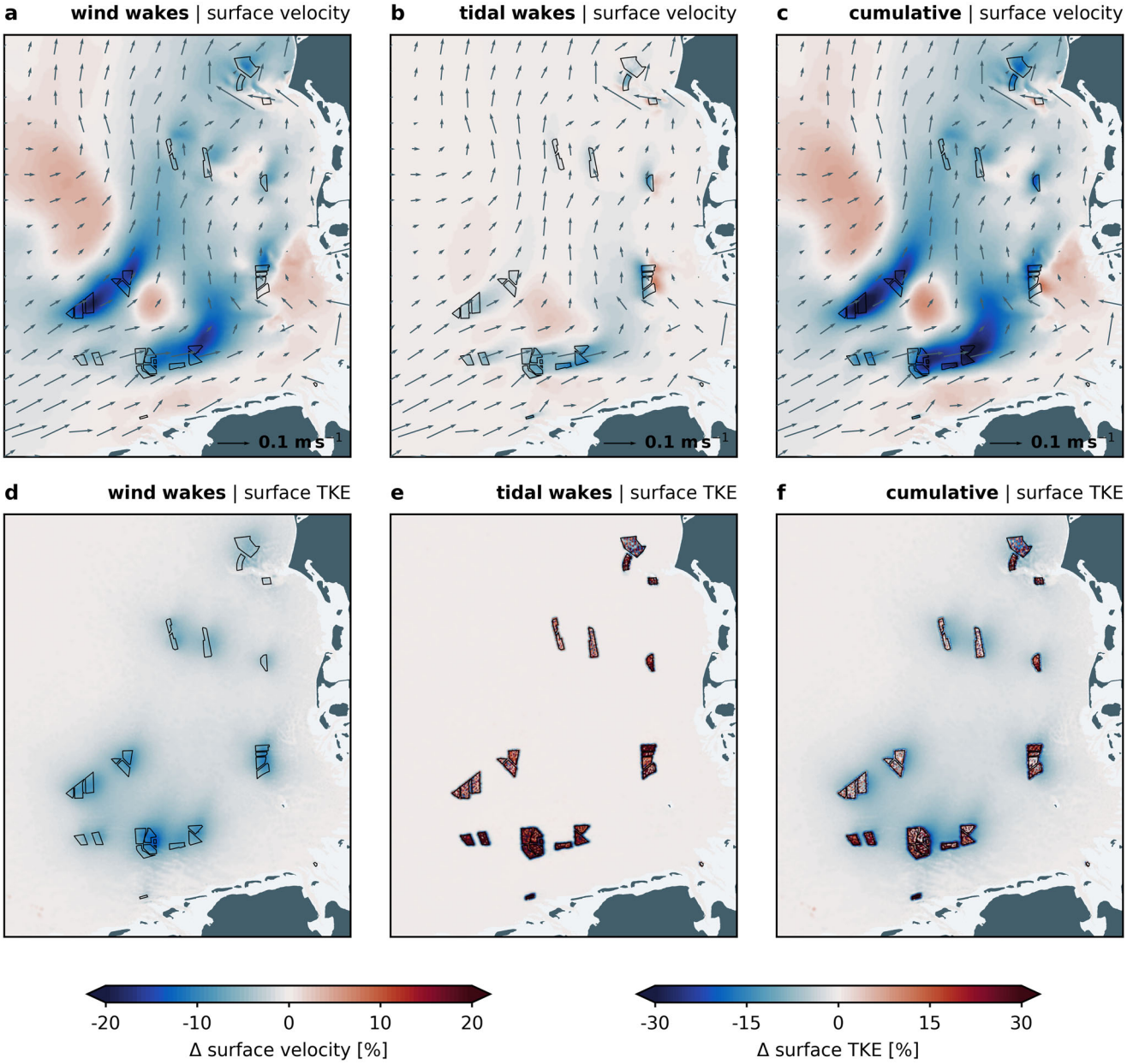

Fig. 1 | Comparison of wind and tidal wake effects. a Temporally averaged changes in horizontal surface velocity (upper 10 m) due to wind speed reductions (2008–2013). Model data is shown for the German Bight (2023 Scenario). Black polygons represent offshore wind farms. Gray arrows indicate mean surface current directions in the control simulation. Water depths shallower than five meters are masked. **b** Temporally averaged changes in horizontal surface velocity due to monopile-induced drag and turbulence. **c** Temporally averaged changes in horizontal surface velocity due to the combined effects of wind speed reduction and monopile-induced drag and turbulence. **d** Temporally averaged changes in surface turbulent kinetic energy (TKE) (upper 10 m) due to wind speed reductions over a period of six years (2008–2013). **e** Temporally averaged changes in TKE due to monopile-induced drag and turbulence. **f** Temporally averaged changes in TKE due to the combined effects of wind speed reduction and monopile-induced drag and turbulence.

mixing rates in the water column are weakest, which is mostly the case during summer months (see Fig. 2a). This suggests that ambient mixing of the water column plays an important role in controlling wind wake effects – a relationship also observed in the context of tides[18].

Overall, the surface temperature anomalies at FINO1 are shaped by strong local mixing in summer and attenuated wind forcing in winter, highlighting the dynamic interaction between wind and tidal wake effects at wind farm sites. Across the densely developed wind farms in the German Bight, tidal wakes emerge as the dominating driver, with the summer SST anomalies (Fig. 2c, and Supplementary Fig. 4) closely linked to the changes in annual mean surface TKE (Fig. 1d–f). Tidal wakes generate localized hotspots of colder mean surface temperature in summer (Supplementary Fig. 4b) that exceed the broader surface warming caused by the reduced wind speeds (Supplementary Fig. 4a). Under the present-day scenario, this pattern results in seasonally averaged surface warming of up to 0.05 °C across the German Bight, accompanied by monopile-induced cooling of up to −0.15 °C or more in direct vicinity of the wind farms.

Cumulative impacts of future offshore wind expansion

Wind and tidal wakes combine to reduce mean current velocities at wind farm sites and downstream. When considering the current and projected future scenarios for offshore wind energy development in the North Sea, the emerging velocity changes create large-scale anomalies in the flow field, here analyzed for a 6-year mean (Fig. 3). The superposition of the wake effects

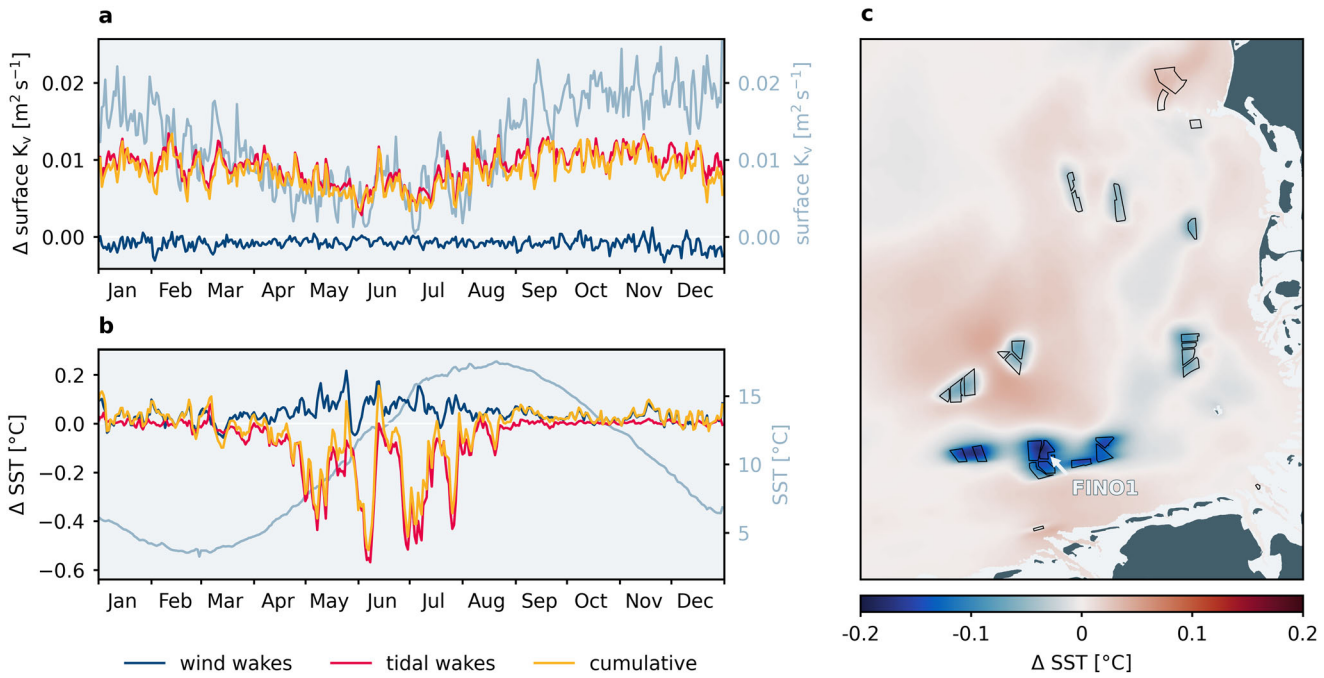

Fig. 2 | Mixing effects caused by wind and tidal wakes. a Mean annual cycle of changes in vertical mixing rate K_v (upper 10 m) at the research platform FINO1 (2008–2013). Blue, red, and yellow lines indicate the time series corresponding to the impact of wind speed reduction (wind wakes), additional turbulence (tidal wakes), and their combination. The undisturbed mixing rates from the control simulation are depicted in light gray in the background. The geographical location of FINO1 is shown in (**c**). **b** Mean annual cycle of changes in sea surface temperature SST (upper 2 m) at the research platform FINO1. The undisturbed surface temperatures from the control simulation are depicted in light gray in the background. **c** Temporally averaged changes in summer SST at wind farm sites (April-August, 2008–2013). Model data is shown for the German Bight (2023 Scenario). Black polygons represent offshore wind farms.

leads to reductions in mean surface velocity of $5-15\%$ on average, corresponding to local changes of around $0.005-0.010\ m\ s^{-1}$. The large-scale velocity reductions are accompanied by increased surface velocities between the wind farm clusters or in areas not occupied by wind turbines, reflecting demonstrated blocking effects of the wind farms[31], which have been also observed in Fig. 1a–c. The patterns and magnitudes of these velocity changes remain highly consistent over the simulated years (Supplementary Fig. 5), indicating the stability of the induced surface current modifications in the southern North Sea.

Considering the recent offshore wind energy development by 2023, the most substantial impacts on surface current velocities occur at wind farms situated near the Dutch and Belgian coast as well as in the German Bight, where turbine densities are highest (Fig. 3a). In these areas, the model suggests long-term velocity reductions of at least 10%. Less pronounced changes can be found in British waters, where wind farms are located further apart, while large parts of the central North Sea remain unaffected.

In contrast, expanding offshore wind energy to a scenario for the year 2050 may have a considerable impact on mean surface velocities distributed across the entire central and southern North Sea (Fig. 3b). For the future scenario, large-scale slowing of the mean surface circulation can be found south of the Dogger Bank from the British coast to the German and Danish waters, with a decrease of at least 5% overall. The model shows velocity reductions on average around $10-15\%$ at wind farm sites and of more than 20% in the German Bight, where presumably the combination of the large number of turbines and the slow residual currents is amplifying the impacts. Conversely, mean surface currents increase north of Dogger Bank due to the large-scale blocking in the wind farm areas. Here, we find continuous positive velocity changes of around 5%, which spread widely across the areas that are not designated for future wind energy production. Similar behavior can also be found near the coastlines in the southern Bight and along the German Wadden Sea area, where mean surface velocity increases by less than 5%.

The overall reduction in mean current velocity originates from the instantaneous changes at wind farm sites, which also manifest in the velocity distribution of hourly surface and bottom currents in the model domain (Fig. 3c). The wake effects cause clear shifts in these distributions, with surface and bottom layer showing an increased frequency of lower velocities and fewer occurrences of higher velocities, indicating a loss in energy in the model domain. In the 2023 scenario, surface velocities above $0.55\ m\ s^{-1}$ become less frequent, likely because most constructed wind farms are located in tidal-dominated coastal areas where the wake effects influence the typically high current speeds in the shallow waters. In the 2050 scenario, however, the shift occurs much earlier at surface velocities above $0.35\ m\ s^{-1}$, as the future wind farms are distributed over much larger parts of the North Sea. In this scenario, the changes in the velocity distribution are also up to five times more pronounced. Meanwhile, bottom currents show a decrease in the frequency of values above $0.10\ m\ s^{-1}$ in both scenarios.

To assess the impact on kinetic energy, we analyze the power spectral density (PSD) of the hourly absolute surface and bottom velocities (Fig. 3d). The PSD changes reveal a redistribution of spectral energy away from the dominant M_2 tide, which decreases by approximately 10% at the surface in both scenarios. The redistribution is likely driven by the large-scale reductions in turbulent kinetic energy, which decrease energy dissipation and thus allow more tidal energy to propagate through the system. As a result, surface and bottom energy is reallocated to both higher- and lower-frequency tidal components. Most notably, the nonlinear overtone $2M_2$ increases due to reduced dissipation and bottom friction. Additional $2M_2$ intensification, along with M_2 reduction, results from enhanced tidal asymmetry. The stronger asymmetry is caused by the tidal influences on the wake effects, which can produce positive or negative velocity changes during flood and ebb conditions[18]. This also amplifies energy in the low-frequency spring-neap cycle (Msf), reinforcing the decline in M_2 dominance.

Overall, signals above the M_2 frequency tend to increase due to the wake effects, while lower-frequency signals largely decrease. While the reduction in M_2 energy is comparable between the two scenarios, the

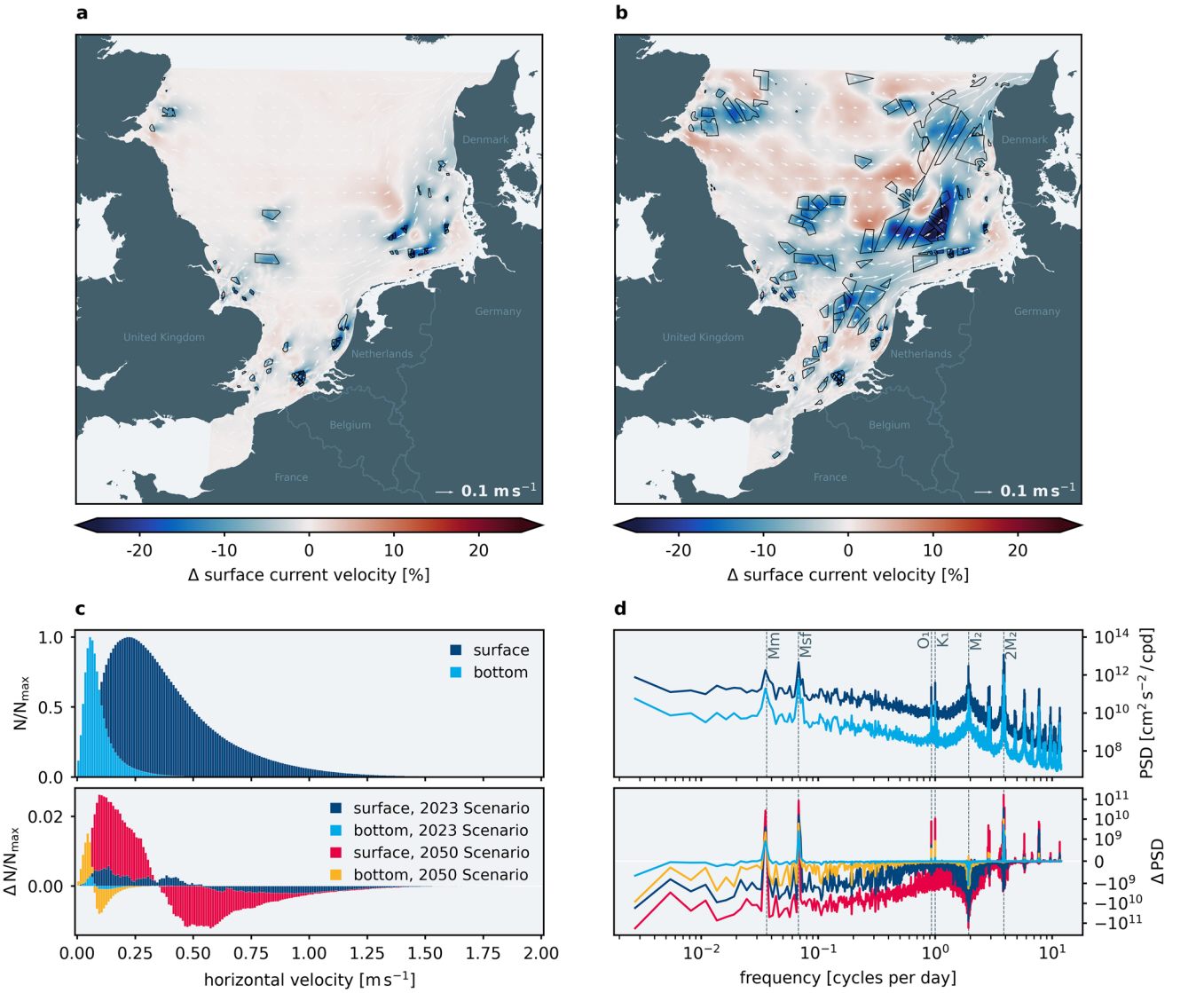

Fig. 3 | Long-term impact on tidal currents. a Changes in temporally averaged surface current velocity (upper 2 m), caused by wind and tidal wakes, for the 2023 Scenario (2008–2013). Black polygons represent offshore wind farms. White arrows indicate the mean surface currents in the control simulation. **b** Changes in temporally averaged surface current velocity for the 2050 Scenario. **c** Normalized distribution of hourly surface and bottom velocities in the model region (upper panel) and the absolute changes caused by the wake effects, divided into the 2023 and 2050 scenarios (lower panel). Data are shown for the first year of the simulations (2008). **d** Power spectral density of hourly surface and bottom velocities and the absolute changes caused by the wake effects. Vertical dashed lines and associated labels indicate dominant tidal frequencies. Data are shown for 2008. The y-axes are logarithmic.

broader spatial impact of the 2050 scenario involves stronger low-frequency responses that are an order of magnitude greater than in the 2023 scenario. Integration over the power spectrum shows a total net kinetic energy loss of 1.5% at the surface and 0.2% at the bottom in the 2023 scenario. In the 2050 scenario, with larger spatial wind farm coverage, these losses increase to 3.7% and 1.4%, respectively. It is important to note that these changes are concentrated near the wind farm locations and are not detectable across the entire model domain. Still, the local alterations strongly influence the total energy budget and result in the extensive velocity anomalies found under future offshore wind expansion (Fig. 3b).

To assess the potential long-term impact of future OWFs and the consequences for hydrodynamic processes, we analyze an extended simulation period of 10 years (2008–2017) in the following.

In the shallow North Sea, the impact of slower surface currents propagates down to the seabed, where the attenuated velocities can influence tidal-induced mixing and bottom shear stress. In particular, the decreasing occurrence of higher velocities near the seabed indicates changes in the bottom shear stress. Here, we identify a large-scale reduction in bottom shear stress of up to 5 − 10% averaged over 10 years (Fig. 4a). Our simulations show the strongest reductions at Dogger Bank and along the Danish west coast, two shallow areas where surface energy can propagate more easily to the seabed and thus bottom shear stress is influenced by both wind and tidal forces[36]. The detected pattern is consistent with previous model results[33], which highlighted the potential large-scale influence of wind wakes on bottom shear stress for a 1-year simulation. Meanwhile, local drag and turbulence generated at the turbine foundations create opposing effects on bottom shear stress and increase it locally by up to 5%. However, this effect is likely underestimated by the model due to the coarse horizontal discretization, which excludes fine-scale processes in between turbines and directly at the foundations. For example, recent in-situ measurements have found that seabed drag at wind turbines can become twice as strong as upstream conditions[24].

The identified changes in bottom currents and shear stress can become critical for erosion and sediment resuspension. Previous studies have shown that extensive wind wake effects can reduce resuspension, leading to a higher amount of organic carbon in seabed sediments near wind farm sites by

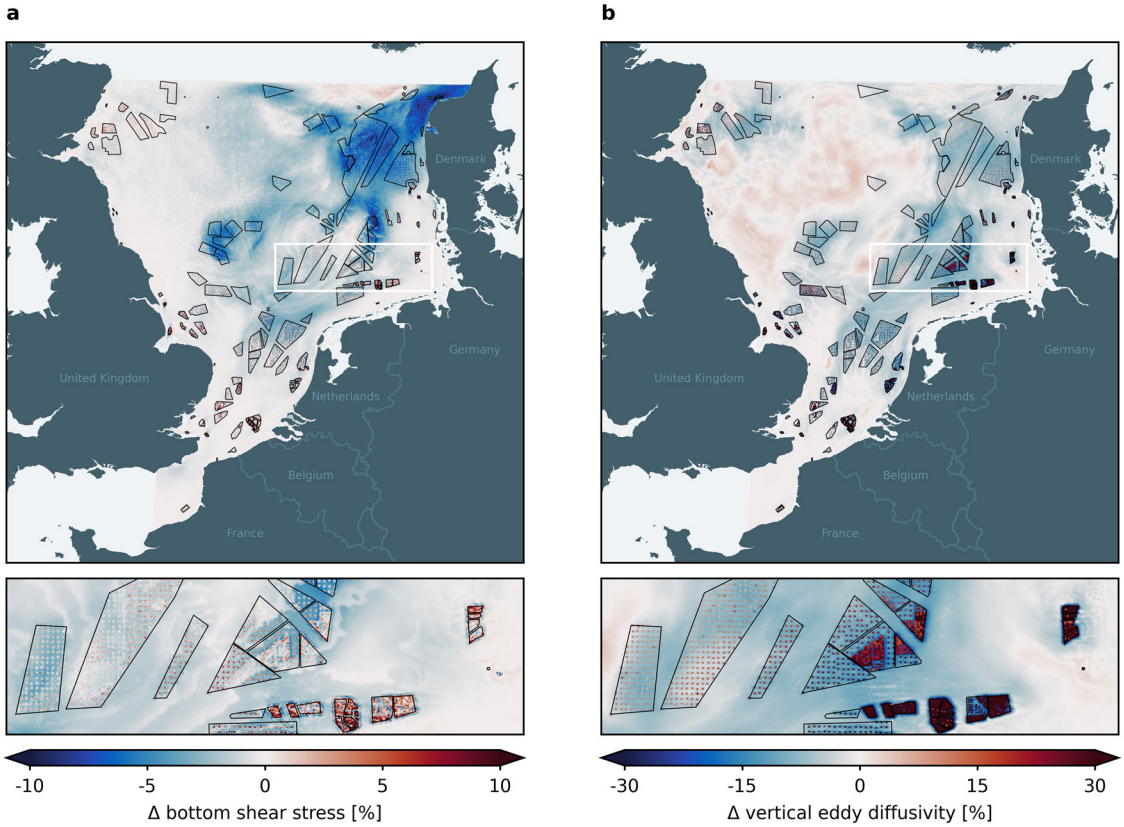

Fig. 4 | Long-term impact on bottom shear and vertical mixing. a Temporally averaged changes in bottom shear (2008–2017). Black polygons represent offshore wind farms. Lower panel shows zoom into German Bight area, indicated by the white dashed box in the upper panel. **b** Temporally averaged changes in depth-averaged vertical eddy diffusivity (vertical mixing).

approximately 10 − 20% [33]. Similarly, wind stress reductions can result in lower suspended sediment concentrations, decreasing light attenuation in the water column and thereby influencing primary production[37]. In contrast, the generated turbulence and bottom shear stress from local monopile drag will increase turbidity at wind farm sites[24,26,27,38,39] and intensify seabed mobility and resuspension. Given the potential large-scale changes in bottom shear stress under future development and the associated impacts on sediment dynamics, more detailed investigations of morphodynamic changes are needed. This also includes high-resolution modeling of the processes inside of wind farms to understand effects on turbulence or sediment transport in-between individual turbines.

The attenuated mean currents and changes in TKE are also reflected in changes to vertical mixing rates. Specifically, we find large-scale reductions in mean vertical mixing in regions where both current velocity and TKE decrease (Fig. 4b). Here, these reductions are around 10% on average, aligning with the identified attenuations in current velocity (Fig. 3b), and are primarily driven by wind wake effects. Conversely, vertical mixing rates increase in regions where we identified stronger residual currents, such as north of Dogger Bank. Near the wind turbines, where TKE is intensified (Supplementary Fig. 6c), vertical mixing rates increase by more than 20% relative to the control simulation. In fact, in high turbine density areas, long-term mixing rates can increase by up to 300% locally. Meanwhile, we find only weak to minor increases in vertical mixing in the future wind farm areas, where we assumed turbine spacings of 3000 m. In these areas, additional mixing does not accumulate and is mitigated by the effects of wind wakes.

Overall, our findings indicate that potential changes in water column mixing can be derived from the combined influence of altered horizontal currents and turbulence. It is important to note, however, that the monthly-averaged mixing values presented here do not capture short-term perturbations and thus do not fully represent instantaneous changes in tidal mixing. Rather, Fig. 4b qualitatively illustrates the spatial distribution of potential increases and decreases in water column mixing under the future development scenario. In this context, the patterns underscore the importance of turbine density, correlated with the magnitude of vertical mixing alterations. In particular, turbine densities of one or more turbines per square kilometer are associated with intensified vertical mixing rates, whereas for lower densities the changes in mixing within wind farms are generally driven by wind stress reductions.

Alterations in surface wind stress and vertical mixing eventually affect mixed-layer dynamics and stratification both within and beyond wind farm boundaries. The ocean's response to wind farm effects is governed by multiple factors, including the relative strength of wind- and tide-driven processes, with strong tidal currents enhancing tidal-wake-induced mixing and promoting destratification, while weaker tidal currents allow wind stress reductions to dominate and increase stratification at wind farm sites[34]. This behavior is reproduced in our simulations and consistent with earlier evidence that strong tidal dynamics mitigate wind wake effects[18].

In our future scenario, the most prominent change is a large-scale increase in mean sea surface temperature SST of approximately 0.05 − 0.15 °C across the model domain (Fig. 5a). These anomalies appear strongly related to the changes in surface current velocity (Fig. 3b, Supplementary Fig. 5d) and vertical mixing (Fig. 4b). The strongest surface warming occurs near wind farms located in seasonally stratified regions of the central North Sea, such as east of Dogger Bank, where mean surface currents are low and wind stress reductions become more relevant. In areas with high turbine densities, persistent mixing mitigates the surface warming by entraining colder bottom water during stratified periods, resulting in colder summer SST (see Fig. 2c). However, we find negative temperature changes in the 10-year average only at a few wind farms in the German Bight, suggesting that the surface temperature response overall is driven by multiple processes rather than solely by changes in vertical mixing.

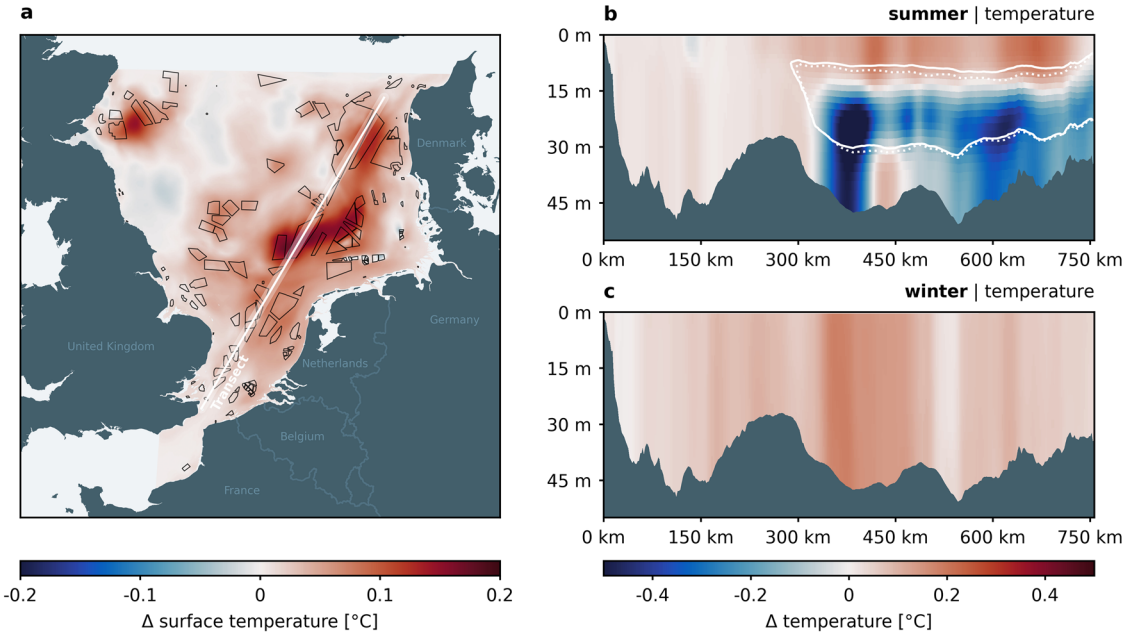

Fig. 5 | Long-term impact on North Sea temperature. a Temporally averaged changes in sea surface temperature (2008–2017). Black polygons represent offshore wind farms. White dashed line indicates transect. **b** Transect of seasonally averaged temperature in summer (June–August, 2008–2017) across offshore wind farm areas from south to north. White contour indicates seasonal pycnocline ($N^2 \geq 5 \times 10^{-5}$ s^{-2}) with wind farms, white dotted contour without wind farms. **c** Transects of seasonally averaged temperature in winter (December-February, 2008–2017).

In general, the heat budget of the ocean's surface mixed layer is controlled by advection, diffusion, mixing, and surface heat fluxes. In the shallow North Sea, where tidal and wind forces dominate, we assume that horizontal advection, mixing processes, and air-sea exchange in particular account for most of the variability. Indeed, spatial correlations reveal strong links between the surface warming and reductions in wind speed and surface currents as well as vertical mixing (Fig. 6c). Additionally, we find that all areas affected by SST anomalies also exhibit changes in heat fluxes, which may represent either drivers of, or feedback to, surface warming (Fig. 6a, b). Air-sea exchange, especially sensible (SH) and latent (LH) heat fluxes, scales with wind speed and surface currents, thus, surface heat fluxes are generally expected to be attenuated by the primary wake effects. However, while the temperature anomalies show strong negative correlations with changes in wind and current speeds, we find that LH changes are positively correlated with wind speed changes and show on average only minor correlation with SST anomalies, in contrast to SH variations (Fig. 6c).

As the monthly-averaged model data prevent closed heat budget calculations for quantitative assessments, we instead examine co-variability between vertical mixing, surface heat fluxes, and surface warming to disentangle the driving processes underlying the SST anomalies (Fig. 6d, e). While most cases of surface warming or cooling can be attributed to changes in mixing, the changes in heat fluxes, and particularly the wind-driven latent heat fluxes, play an equally important role. When surface mixing decreases and surface temperature increases, enhanced surface warming is typically accompanied by stronger upward heat fluxes, especially through sensible heat losses to the atmosphere (Fig. 6c, e). While this process is associated with the strongest SST anomalies in the model, we find in many cases, however, that net heat fluxes decrease despite rising SST. This suggests that reduced wind and current speeds weaken the air-sea exchange, thereby reducing heat loss and contributing to surface warming. This mechanism occurs especially in well-mixed regions and during winter months, when air-sea exchange exerts stronger control on the surface heat budget than vertical mixing, allowing reduced wind-driven LH fluxes to cause surface warming even under enhanced mixing conditions (Fig. 6d). In contrast, in seasonally stratified waters, reduced mixing remains the dominant driver of SST anomalies, as stratification changes directly affect the surface layer heat balance and heat fluxes primarily respond to, rather than drive, the resulting warming (Fig. 6a).

The identified relationship between mixing and heat flux changes, and its dependence on stratification strength, results in pronounced spatial and seasonal variability in their effects on water temperature and density. The most substantial impact on temperature occurs during summer, when the reduced surfaces mixing enhances stratification in seasonally stratified regions. Here, we find temperature changes between −0.6 °C and 0.2 °C along a transect across the model domain, with positive changes near the surface and negative changes below the pycnocline (Fig. 5b). The largest temperature reductions occur just below the surface mixed layer, indicating shifts in the thermocline structure due to reduced vertical entrainment. Thereby, the pycnocline depth is reduced by up to two meters relative to the control simulation. The most pronounced impact on temperature stratification occurs near Oyster Ground (~ 350 km of transect, Fig. 5b), a region linked to low bottom oxygen concentrations[40] and potentially at risk of bottom deoxygenation due to the impact of wind wakes[33]. Our results suggest that such conditions are favored by the increased stratification found here (Supplementary Fig. 6d). Meanwhile, in well-mixed regions of the model domain as well as during winter months, the model shows consistently higher temperatures throughout the vertical transect (Fig. 5c). This overall warming reflects the net increase in ocean heat budget caused by the modified surface heat fluxes and limited heat loss. Notably, the winter temperature changes are comparable in magnitude to the surface warming in summer, emphasizing that heat fluxes are a primary factor in the temperature response to wind wake effects, particularly in mixed waters.

The long-term increase in annual sea surface temperature on the order of 0.1 °C remains within the natural interannual variability of approximately 1 °C[41]. Nevertheless, this induced surface warming mimics the influence of global warming and reaches magnitudes of roughly 10% of projected climate change signals in the North Sea (1 − 3 °C[42,43]). Regional atmospheric modeling has shown that wind wakes can increase annual-mean near-surface temperature in the North Sea by about 0.1 °C[12], which may further amplify the simulated surface warming in our study. Beyond environmental consequences from surface warming, identified changes in air-sea heat fluxes and SST may feed back on the near-surface climate and the development of wind wakes, which are highly sensitive to atmospheric

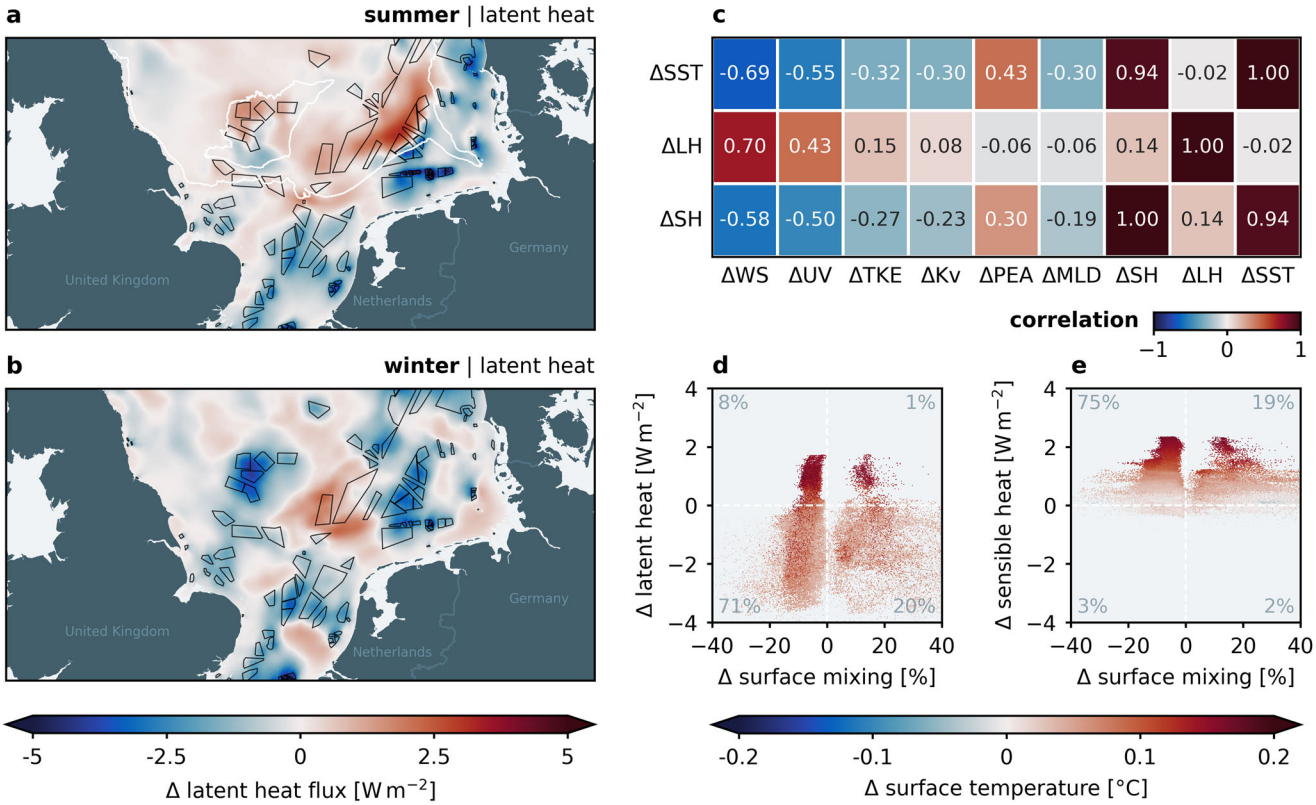

Fig. 6 | Correlations between surface warming and surface heat fluxes. **a** Temporally averaged changes in latent heat flux in summer (June–August, 2008–2017). Black polygons represent offshore wind farms. White lines indicate the mean 20 J m^{-3} contour in summer, representing the transition from well-mixed to stratified waters. **b** Temporally averaged changes in latent heat flux in winter (December–February). **c** Correlation matrix between averaged changes in sea surface temperature (SST), latent heat flux (LH), and sensible heat flux (SH), and a set of physical variables: wind speed (WS), horizontal velocity (UV), turbulent kinetic energy (TKE), vertical mixing (Kv), potential energy anomaly (PEA), and mixed layer depth (MLD). **d** Scatter density plot of averaged changes in latent heat at wind farm sites as a function of the relative change in vertical mixing in the surface layer (upper 5 m). Colors indicate the corresponding temperature anomalies. Percent values denote the fraction of data points in each quadrant. **e** Scatter density plot of averaged changes in sensible heat flux at wind farm sites as a function of the relative change in vertical mixing in the surface layer.

boundary layer stability[5,6,10]. Recent fully coupled atmosphere-ocean simulations have demonstrated that wind-wake-induced surface warming can locally enhance both 10-m wind speed and surface wind stress[44]. Building on these findings, similar coupled modeling approaches are required in the North Sea to resolve feedback between hydrographic changes and atmospheric OWF effects and to assess the full impact from wind wakes.

Ultimately, the induced impacts from OWF wakes are directly linked to the North Sea's seasonal stratification, which shows strong feedback from the changes in vertical mixing. For instance, areas of intensified mixing in the German Bight weaken seasonal stratification, whereas attenuated surface mixing, such as near Dogger Bank, can enhance the stratification strength (Supplementary Fig. 6d). In both cases, these local perturbations can cause lateral shifts in the mean pycnocline and thus modify mixing fronts, with changes in potential energy changes (up to ±5 J m^{-3}) comparable in magnitude to those projected under climate change scenarios in these regions[42]. Such impacts on stratification are likely to play a critical role in shaping lower trophic ecosystem dynamics, as stratification naturally controls nutrient transport in the water column[45]. Previous studies have shown that a shallower mixed layer depth due to wind wakes can shift the vertical production maximum upward in deep, stratified waters[33]. In contrast, in less-stratified waters, increased stratification may suppress primary production due to a stronger natural barrier.

Interpretation and contextualization of the model results

The hydrodynamics of the North Sea are governed by wind and tidal forces, both of which are modified by the cumulative effects of OWFs. While wind farms perturb a range of wind- and tide-driven processes, our model simulations indicate that, on long time scales, the response of this highly dynamic system is dominated by changes in shear-driven mixing and residual circulation, arising from regional reductions in wind stress and localized turbulence hotspots. Wind wakes emerge as the main driver of the large-scale hydrodynamic footprint, reducing surface layer turbulence and air-sea fluxes. Tidal wakes can locally counteract turbulence reductions but reinforce impacts on residual circulation. Future expansion of offshore wind energy may propagate these effects across the North Sea and into stratified waters, with potential implications for biogeochemistry and lower-trophic ecosystem dynamics.

In interpreting our model results, it should be noted that methodological and scenario-related uncertainties exist. For example, wind wakes are represented using a simplified parameterization that does not explicitly account for atmospheric stability, effects on surface climate, or individual wind farm capacities. Likewise, the parameterization of monopile-induced turbulence relies on predefined mixing coefficients that determine the additional local turbulence production. These assumptions may lead to over- or underestimation of the quantitative responses. However, the driving mechanisms are expected to remain robust, as they are consistent with recent studies. For example, mean surface wind speed reductions and spatial impact patterns are in good agreement with more advanced modeling approaches that resolve atmospheric dynamics more explicitly[12,33,34].

Individual wind turbines create small, localized impacts on ocean dynamics; however, the accumulation of these effects can become substantial at wind farm scale. The hydrodynamic footprint proves to be site-specific and depends on hydrographic conditions and wind farm properties, with turbine density emerging as a critical control. In our simulations,

turbine spacings of about 3000 m produce only minor accumulated turbulence, whereas spacings of 1000 m or less generate pronounced hotspots of vertical mixing and enhanced current-blocking effects. These findings are consistent with idealized simulations, showing that velocity reductions at widely spaced wind farms, such as those at Dogger Bank, can be an order of magnitude lower than in more densely spaced installations in the German Bight[31]. Similarly, atmospheric modeling showed that deploying larger turbines with greater spacing can mitigate the impact of wind wakes on surface climate and wind speed[35]. These findings indicate that increasing turbine spacing offers a practical pathway to reduce the hydrodynamic footprint of OWFs.

Our results highlight that the hydrodynamic response to wake effects is strongly conditioned by the underlying tidal regime, which sets the background state against which induced perturbations act. Reductions of horizontal currents and changes in vertical mixing emerge as key drivers, while the model also indicates that changes in surface heat fluxes play a decisive role. The relative importance of these drivers depends on tidal preconditioning of the water column. In stratified waters, where tidal mixing is weaker, wind-farm-induced changes in mixing dominate by directly altering stratification. In contrast, tidally energetic, well-mixed regions respond predominantly to changes in wind-driven air-sea exchange, as strong background mixing limits the sensitivity of the vertical density structure to additional turbulence. The pronounced influence of surface heat fluxes underscores the need for three-dimensional atmospheric modeling of wind wakes or even coupled ocean-atmosphere simulations to capture the holistic impacts and feedback from wind wakes accurately and to account for atmospheric effects on near-surface temperature and humidity[12,44].

In the North Sea, most operating wind farms are located in regions that are tidally mixed year-round or stratified only seasonally. In this environment, the thermal response is primarily governed by wind-wake-induced changes in latent heat flux and air-sea exchange, while changes in vertical mixing become more relevant during summer stratification, when they can affect stratification strength and timing. Future expansion of OWFs into persistently stratified regions is therefore likely to increase the relative importance of mixing-driven responses, particularly under additional climate-driven intensification of stratification.

Although the magnitude and spatial extent of impacts remain site-specific, our findings can provide a framework for interpreting OWF effects in other coastal seas. In strongly tide-dominated regions, air-sea exchange and current-blocking effects are expected to be the primary control where the water column is mixed and tidal currents are high. In stratified regions, mixing alterations and impacts on vertical density structure are likely among the primary drivers. Along the seasonally stratified U.S. North Atlantic shelf, for example, wind wakes have been shown to induce changes in vertical entrainment cooling, coastal upwelling, and surface layer mixing, leading to surface warming and modifying stratification[44]. Collectively, these results highlight the complex interplay of vertical mixing, air-sea exchange, and tidal dynamics in shaping the hydrographic footprint of OWFs and the importance of local hydrodynamic conditions.

Methods

Model description and setup

For 3D hydrodynamic modeling the Semi-implicit Cross-scale Hydroscience Integrated System Model (SCHISM)[46] has been used, which employs a semi-implicit finite-element/finite-volume method to solve the Reynolds-averaged Navier-Stokes equations under hydrostatic and Boussinesq approximations. SCHISM is based on a customizable unstructured horizontal triangular grid that allows for flexible local grid refinement, enabling high resolution of targeted processes and areas, while resolving larger scale ocean circulation at more efficient grid resolution. Here, the model setup was built upon a validated model system for the central North Sea presented in earlier studies[13,18], but was extended for longer time periods and adapted for the different offshore wind scenarios. Transport equations were solved with a Total Variation Diminishing advection scheme in the horizontal and vertical, and turbulence was calculated using the Generic Length-Scale formulation[47] with the $k-\varepsilon$ model.

The model setup has open boundaries in the English Channel and at the transition to the northern North Sea between Scotland and Denmark. At its open boundaries, the model was driven by daily averaged reanalysis data for the North-West European Shelf (obtained from EU Copernicus Marine Service (https://doi.org/10.48670/moi-00059), downloaded in February 2023), providing temperature and salinity as well as horizontal velocities and surface height. Furthermore, the model was forced by hourly atmospheric data and considered daily river discharge from the land boundaries. For tidal forcing, eight tidal constituents (M_2, S_2, K_2, N_2, K_1, O_1, Q_1, P_1) were taken into account. The time step of the model simulations was 120*s*. More details on the model setup can be found in Christiansen et al.[13].

In comparison to the previous model setup, horizontal and vertical grid resolution were adjusted for more computational efficiency here. We used grid spacing of 700 m in coastal areas and 2000 m in the open sea, with a depth-dependent linear increase between. At small rivers along the land boundaries the grid spacing could go down to 100 m to resolve river channels properly. OWF areas were resolved with a grid resolution of 700 m locally and at least 1000 m within a 10-km radius of each wind farm (Supplementary Fig. 2). The vertical grid had a maximum of 46 layers and was discretized with depth-dependent flexible Localized Sigma Coordinates[48].

The former model setup demonstrated good skill in reproducing surface salinities, temperatures, and summer stratification patterns[13]. This also holds for the adapted configuration used in the present study. The model successfully generates the characteristic seasonal stratification in the central North Sea (Supplementary Fig. 3a), which is essential for the subsequent impact analyzes of OWF wakes. It performs well in reproducing tidal elevations and phases, as well as daily sea level trends (Supplementary Fig. 3b, c). Moreover, the model captures the seasonal variability of sea surface temperature and salinity at the FINO1 station, located within an OWF area in the German Bight (Supplementary Fig. 3d, f). Comparisons with the well-established Copernicus reanalysis data, used at the open boundaries, indicate that simulated temperature and salinity fields represent the main hydrographic features of the central and southern North Sea (Supplementary Fig. 3e, g). Although the model tends to be slightly too diffusive and underestimate stratification, it provides a robust basis for detailed process analyzes of potential OWF impacts under typical North Sea conditions.

Model experiments

Various model experiments were conducted in this study, divided into three scenarios: (i) a control scenario, (ii) a 2023 offshore wind scenario, and (iii) a 2050 offshore wind scenario. All simulations were performed as hindcasts for the period 2008–2013 or 2008–2017, respectively (see Table 1). The control simulation represents reference conditions without OWF effects. The 2023 and 2050 scenarios account for the physical effects of offshore wind turbines based on technical layouts for 2023 and projected 2050 installations, respectively. These effects included surface wind speed reductions behind wind farms as well as additional underwater drag and turbulence at turbine sites, which were parameterized in the SCHISM model.

The scenario development and assumptions made for 2023 and 2050 installations are based on the *4C Offshore* database (https://www.4coffshore.com/windfarms/, as of March 02, 2023). In the 2023 scenario, we considered all OWFs in the central North Sea, which were in operation or under construction in the beginning of 2023 (Supplementary Fig. 1a). For the 2050 scenario, we have used all available development areas in the central North Sea, i.e., existing, planned or projected, which combined resulted in a total production capacity of approximately the targeted 300 GW by 2050 (Supplementary Fig. 1b).

All model experiments were initiated from a 2-year spin-up simulation. For the 2023 scenario, we performed three separate hindcast simulations to examine the effects of wind and tidal wakes both individually and

Table 1 | List of model experiments grouped into offshore wind scenarios

Scenario	Simulation period	Grid configuration	OWF effects
spin-up	01/2006–12/2007	Default	–
control	01/2008–12/2017	OWF 2023, OWF 2050	–
2023	01/2008–12/2013	OWF 2023	Wind wakes, tidal wakes & combination
2050	01/2008–12/2017	OWF 2050	Combination of wind and tidal wakes

collectively over a period of 6 years (2008–2013). For the 2050 scenario, we extended the simulations to a 10-year period (2008–2017) and focused only on the cumulative effect of wind and tidal wakes. The model grid has been adjusted for each scenario, considering the respective offshore wind areas in 2023 and 2050. For each offshore wind experiment, we performed an individual control simulation with the respective grid configuration. An overview of all performed model experiments is given in Table 1. Model experiments provided daily and monthly output day for the 2023 scenario and monthly data for the 2050 scenario.

For the model analysis, we looked at the relative and absolute differences between the offshore wind experiments (OWF) and the control simulations (CTL):

$$\Delta = \mathrm{OWF} - \mathrm{CTL} \tag{1}$$

Parameterization of offshore wind farm effects

Wind wakes and tidal wakes have been implemented into the hydrostatic SCHISM model using validated parameterizations for surface wind speed reductions and monopile-induced drag and turbulence. The parameterizations are integrated as additional modules that can be activated as needed.

The wind wakes are described by a simplified empirical wake model developed by Christiansen et al.[13], which treats OWF polygons as a single unit and alters the undisturbed surface wind speed u_0 by an exponential velocity deficit Δu in downstream direction. Here, we added a new term to describe the buildup of the wind speed reduction inside the wind farm area. This additional term is inspired by Broström et al.[14] and consistent with observations from recent atmospheric modeling[7,12].

$$u_r(x,y) = u_0\left(1 - \Delta u(x,y)\right) \tag{2}$$

$$\Delta u(x,y) = \begin{cases} \alpha \cdot e^{-\frac{x-x_0}{\sigma} - \frac{y^2}{\gamma^2}}, \text{if} x \geq x_0 \\ \alpha \cdot e^{\frac{x-x_0}{x_0} - \frac{y^2}{\gamma^2}}, \text{if} x < x_0 \end{cases} \tag{3}$$

In the parameterization, x and y denote the longitudinal and cross directions in the rotated coordinate system, which is aligned with the respective upstream wind direction, and x_0 represents the wind farm boundary in the direction of flow. The model parameters determine the maximum wind speed reduction in percent (α), the recovery of the downstream wind speed (σ), and cross-sectional wake shape (γ). Here, we used $\alpha = 10\%$ and $\sigma = 30$ km, while γ is proportional to the width of the wind farm.

Tidal wakes are described by a subgrid-scale parameterization for drag and turbulence created by monopile foundations, originally introduced by Rennau et al.[19] and implemented into SCHISM by Christiansen et al.[32]. This approach uses the horizontal drag per grid cell $\mathbf{F_d}$ that a vertical cylinder exerts on the horizontal flow, expressed by

$$\mathbf{F_d} = \frac{1}{2} N C_d \frac{d}{A} |\mathbf{u}| \mathbf{u}, \tag{4}$$

where N is the number of monopiles per grid cell, C_d is the drag coefficient, d is the diameter of the monopile, A is the horizontal area of the grid cell, and $\mathbf{u}$ is the velocity of the free stream. This drag force was added to the momentum and turbulence closure equations of SCHISM and applied if a model grid cell contained wind turbines. Turbines themselves are not physically represented in the model grid. Here, we used $C_d = 0.63$ and $d = 8m$ for all wind turbines (Table 2).

Table 2 | Offshore wind turbine information for the present and future scenario

Scenario 2023			
Number of wind farms	Number of turbines	Turbine foundations	Turbine parameters
76	4699	monopiles	$d = 8m, C_d = 0.63$
Scenario 2050			
Number of wind farms	Number of turbines	Turbine foundations	Turbine parameters
146	10159	monopiles	$d = 8m, C_d = 0.63$

We obtained the required turbine locations from the *4C Offshore* database, if available. For future wind farm areas without turbine information, we assumed fixed turbine spacings depending on the size of a wind farm and filled the wind farms with hypothetical turbines in a grid pattern. Based on existing turbine density information from the *4C Offshore* database, we selected a turbine spacing of 1000 m for wind farms with an area of under 20 km^2, a spacing of 3000 m for wind farm areas with an area over 60 km^2, and 1500 m otherwise. The average spacing of the existing turbines installed by 2023 was around 900 − 1300 m.

Data availability

The model data used and/or analyzed in the current study are publicly available at https://doi.org/10.5281/zenodo.18031484.

Received: 16 July 2025; Accepted: 5 January 2026;
Published online: 13 January 2026

References

1. Ostend Declaration on the North Seas as Europe's Green Power Plant. Federal Ministry for Economic Affairs and Climate Action (BMWK), Germany. https://www.bmwk.de/Redaktion/DE/Downloads/Energie/ostend-declaration-energy-ministers-north-seas-europes-green-power-plant.html (2023).
2. Fitch, A. C. et al. Local and mesoscale impacts of wind farms as parameterized in a mesoscale NWP model. *Mon. Weather Rev.* **140**, 3017–3038 (2012).
3. Emeis, S. et al. T. Exploring the wakes of large offshore wind farms. *J. Phys. Conf. Ser.* **753**, 092014 (2016).
4. Platis, A. et al. First in situ evidence of wakes in the far field behind offshore wind farms. *Sci. Rep.* **8**, 2163 (2018).
5. Platis, A. et al. Long-range modifications of the wind field by offshore wind parks – results of the project WIPAFF. *Meteorol. Z.* **29**, 355–376 (2020).
6. Cañadillas, B. et al. Offshore wind farm wake recovery: airborne measurements and its representation in engineering models. *Wind Energy* **23**, 1249–1265 (2020).

7. Akhtar, N., Geyer, B., Rockel, B., Sommer, P. S. & Schrum, C. Accelerating deployment of offshore wind energy alter wind climate and reduce future power generation potentials. *Sci. Rep.* **11**, 11826 (2021).
8. Frandsen, S. et al. Analytical modelling of wind speed deficit in large offshore wind farms. *Wind Energy* **9**, 39–53 (2006).
9. Christiansen, M. B. & Hasager, C. B. Wake effects of large offshore wind farms identified from satellite SAR. *Remote Sens. Environ.* **98**, 251–268 (2005).
10. Djath, B., Schulz-Stellenfleth, J. & Cañadillas, B. Impact of atmospheric stability on X-band and C-band synthetic aperture radar imagery of offshore windpark wakes. *J. Renew. Sustain. Energy* **10**, 043301 (2018).
11. Hasager, C. B. et al. Using satellite SAR to characterize the wind flow around offshore wind farms. *Energy* **8**, 5413–5439 (2015).
12. Akhtar, N., Geyer, B. & Schrum, C. Impacts of accelerating deployment of offshore windfarms on near-surface climate. *Sci. Rep.* **12**, 18307 (2022).
13. Christiansen, N., Daewel, U., Djath, B. & Schrum, C. Emergence of large-scale hydrodynamic structures due to atmospheric offshore wind farm wakes. *Front. Mar. Sci.* **9**, 818501 (2022).
14. Broström, G. On the influence of large wind farms on the upper ocean circulation. *J. Mar. Syst.* **74**, 585–591 (2008).
15. Paskyabi, M. B. & Fer, I. Upper ocean response to large wind farm effect in the presence of surface gravity waves. *Energy Proc.* **24**, 245–254 (2012).
16. Ludewig, E. *On the Effect of Offshore Wind Farms on the Atmosphere and Ocean Dynamics* (Springer Cham, 2015). https://doi.org/10.1007/978-3-319-08641-5.
17. Floeter, J., Pohlmann, T., Harmer, A. & Möllmann, C. Chasing the offshore wind farm wind-wake-induced upwelling/downwelling dipole. *Front. Mar. Sci.* **9**, 884943 (2022).
18. Christiansen, N., Daewel, U. & Schrum, C. Tidal mitigation of offshore wind wake effects in coastal seas. *Front. Mar. Sci.* **9**, 1006647 (2022).
19. Rennau, H., Schimmels, S. & Burchard, H. On the effect of structure-induced resistance and mixing on inflows into the Baltic Sea: a numerical model study. *Coast. Eng.* **60**, 53–68 (2012).
20. Carpenter, J. R. et al. Potential impacts of offshore wind farms on North Sea stratification. *PLoS ONE* **11**, e0160830 (2016).
21. Grashorn, S. & Stanev, E. V. Kármán vortex and turbulent wake generation by wind park piles. *Ocean Dyn.* **66**, 1543–1557 (2016).
22. Rogan, C., Miles, J., Simmonds, D. & Iglesias, G. The turbulent wake of a monopile foundation. *Renew. Energy* **93**, 180–187 (2016).
23. Miles, J., Martin, T. & Goddard, L. Current and wave effects around windfarm monopile foundations. *Coast. Eng.* **121**, 167–178 (2017).
24. Austin, M. J., Unsworth, C. A., Van Landeghem, K. J. J. & Lincoln, B. J. Enhanced bed shear stress and mixing in the tidal wake of an offshore wind turbine monopile. *Ocean Sci.* **21**, 81–91 (2025).
25. Li, X., Chi, L., Chen, X., Ren, Y. & Lehner, S. SAR observation and numerical modeling of tidal current wakes at the East China Sea offshore wind farm. *J. Geophys. Res. Oceans* **119**, 4958–4971 (2014).
26. Vanhellemont, Q. & Ruddick, K. Turbid wakes associated with offshore wind turbines observed with Landsat 8. *Remote Sens. Environ.* **145**, 105–115 (2014).
27. Bailey, L. P. et al. Monopile-induced turbulence and sediment redistribution form visible wakes in offshore wind farms. *Front. Earth Sci.* **12**, 1383726 (2024).
28. Floeter, J. et al. Pelagic effects of offshore wind farm foundations in the stratified North Sea. *Prog. Oceanogr.* **156**, 154–173 (2017).
29. Schultze, L. K. P., Merckelbach, L. M., Horstmann, J., Raasch, S. & Carpenter, J. R. Increased mixing and turbulence in the wake of offshore wind farm foundations. *J. Geophys. Res. Oceans* **125**, e2019JC015858 (2020).
30. Dorrell, R. M. et al. Anthropogenic mixing in seasonally stratified shelf seas by offshore wind farm infrastructure. *Front. Mar. Sci.* **9**, 830927 (2022).
31. Carpenter, J. R. & Guha, A. Blocking effects on mean ocean currents by offshore wind farm foundations. *Phys. Rev. Fluids* **9**, 103802 (2024).
32. Christiansen, N., Carpenter, J. R., Daewel, U., Suzuki, N. & Schrum, C. The large-scale impact of anthropogenic mixing by offshore wind turbine foundations in the shallow North Sea. *Front. Mar. Sci.* **10**, 1178330 (2023).
33. Daewel, U., Akhtar, N., Christiansen, N. & Schrum, C. Offshore wind farms are projected to impact primary production and bottom water deoxygenation in the North Sea. *Commun. Earth Environ.* **3**, 292 (2022).
34. Maar, M. et al. Spatial impacts of offshore wind farms on hydrodynamics and biogeochemical environment. *Aarhus University, DCE – Danish Centre for Environment and Energy*, 70 pp. Scientific Report No. 658 https://dce.au.dk/fileadmin/dce.au.dk/Udgivelser/Videnskabelige_rapporter_600-699/SR658.pdf (2025).
35. Akhtar, N., Geyer, B. & Schrum, C. Larger wind turbines as a solution to reduce environmental impacts. *Sci. Rep.* **14**, 6608 (2024).
36. Wilson, R. J. & Heath, M. R. Increasing turbidity in the North Sea during the 20th century due to changing wave climate. *Ocean Sci.* **15**, 1615–1625 (2019).
37. van der Molen, J., Smith, H. C. M., Lepper, P., Limpenny, S. & Rees, J. Predicting the large-scale consequences of offshore wind turbine array development on a North Sea ecosystem. *Cont. Shelf Res.* **85**, 60–72 (2014).
38. Baeye, M. & Fettweis, M. In situ observations of suspended particulate matter plumes at an offshore wind farm, southern North Sea. *Geo-Mar. Lett.* **35**, 247–255 (2015).
39. Forster, R. M. *The Effect of Monopile-Induced Turbulence on Local Suspended Patterns around UK Wind Farms: Field Survey Report*. An IECS report to The Crown Estate. ISBN 978-1-906410-77-3 https://cms.ore.catapult.org.uk/wp-content/uploads/2018/12/The-Effect-of-Monopile-Induced-Turbulence-on-Local-Suspended-Sediment-Pattern-around-UK-Wind-Farms.pdf (2018).
40. Weston, K. et al. Sedimentary and water column processes in the Oyster Grounds: a potentially hypoxic region of the North Sea. *Mar. Environ. Res.* **65**, 235–249 (2008).
41. Daewel, U. & Schrum, C. Low-frequency variability in North Sea and Baltic Sea identified through simulations with the 3-D coupled physical–biogeochemical model ECOSMO. *Earth Syst. Dyn.* **8**, 801–815 (2017).
42. Schrum, C. et al. Projected change—North Sea. In *North Sea Region Climate Change Assessment. Regional Climate Studies* (eds Quante, M. & Colijn, F.) (Springer Cham, 2016). https://doi.org/10.1007/978-3-319-39745-0_6.
43. Tinker, J., Lowe, J., Pardaens, A., Holt, J. & Barciela, R. Uncertainty in climate projections for the 21st century northwest European shelf seas. *Prog. Oceanogr.* **148**, 56–73 (2016).
44. Seo, H., Sauvage, C., Renkl, C., Lundquist, J. K. & Kirincich, A. Sea surface warming and ocean-to-atmosphere feedback driven by large-scale offshore wind farms under seasonally stratified conditions. *Sci. Adv.* **11**, eadw7603 (2025).
45. Simpson, J. H. & Sharples, J. *Introduction to the Physical and Biological Oceanography of Shelf Seas*. (Cambridge University Press, Cambridge, 2012). https://doi.org/10.1017/CBO9781139034098.
46. Zhang, Y. J., Ye, F., Stanev, E. V. & Grashorn, S. Seamless cross-scale modeling with SCHISM. *Ocean Model.* **102**, 64–81 (2016).
47. Umlauf, L. & Burchard, H. A generic length-scale equation for geophysical turbulence models. *J. Mar. Res.* 235–265 https://doi.org/10.1357/002224003322005087 (2003).
48. Zhang, Y. J., Ateljevich, E., Yu, H.-C., Wu, C. H. & Yu, J. C. S. A new vertical coordinate system for a 3D unstructured-grid model. *Ocean Model.* **85**, 16–31 (2015).

Acknowledgements
We thank the reviewers and editors for constructive reviews, which helped to improve this paper. This study is a contribution to the EXC 2037 'Climate, Climatic Change, and Society (CLICCS)' (Project Number: 390683824) funded by the German Research Foundation (DFG), to the CLICCS-HGF networking project funded by the Helmholtz Association of German Research Centers (HGF), and to the Helmholtz Research Program "Changing Earth – Sustaining our Future", Topic 4. Furthermore, this work contributes to the DAM Research Mission sustainMare and the project CoastalFutures I (Project Number: 03F0911A) funded by the German Federal Ministry of Research, Technology and Space (BMFTR, formerly known as Federal Ministry of Education and Research (BMBF)).

Author contributions
N.C. conceived the study, designed the study setup, performed the model simulations and data analysis, and prepared the manuscript and figures. U.D. and C.S. contributed to the data analysis, the discussion and the study design. All authors contributed to manuscript writing and approved the final version.

Funding
Open Access funding enabled and organized by Projekt DEAL.

Competing interests
The authors declare no competing interests.

Additional information
Supplementary information The online version contains supplementary material available at https://doi.org/10.1038/s43247-026-03186-8.

Correspondence and requests for materials should be addressed to Nils Christiansen.

Peer review information *Communications Earth and Environment* thanks Zhaoqing Yang and the other, anonymous, reviewer(s) for their contribution to the peer review of this work. Primary Handling Editors: Olusegun Dada and Alice Drinkwater. [A peer review file is available].